

Article

Performance Assessment of a Solar-Assisted Desiccant-Based Air Handling Unit Considering Different Scenarios

Giovanni Angrisani, Carlo Roselli, Maurizio Sasso, Francesco Tariello * and Giuseppe Peter Vanoli

Department of Engineering, University of Sannio, Piazza Roma 21, Benevento 82100, Italy; gangrisa@unisannio.it (G.A.); carlo.roselli@unisannio.it (C.R.); sasso@unisannio.it (M.S.); vanoli@unisannio.it (G.P.V.)

* Correspondence: tariellofrancesco86@gmail.com; Tel.: +39-0824-305576; Fax: +39-0824-325246

Academic Editor: Tapas Mallick

Received: 21 June 2016; Accepted: 30 August 2016; Published: 8 September 2016

Abstract: In this paper, three alternative layouts (scenarios) of an innovative solar-assisted hybrid desiccant-based air handling unit (AHU) are investigated through dynamic simulations. Performance is evaluated with respect to a reference system and compared to those of the innovative plant without modifications. For each scenario, different collector types, surfaces and tilt angles are considered. The effect of the solar thermal energy surplus exploitation for other low-temperature uses is also investigated. The first alternative scenario consists of the recovery of the heat rejected by the condenser of the chiller to pre-heat the regeneration air. The second scenario considers the pre-heating of regeneration air with the warmer regeneration air exiting the desiccant wheel (DW). The last scenario provides pre-cooling of the process air before entering the DW. Results reveal that the plants with evacuated solar collectors (SC) can ensure primary energy savings (15%–24%) and avoid equivalent CO₂ emissions (14%–22%), about 10 percentage points more than those with flat-plate collectors, when the solar thermal energy is used only for air conditioning and the collectors have the best tilt angle. If all of the solar thermal energy is considered, the best results with evacuated tube collectors are approximately 73% in terms of primary energy saving, 71% in terms of avoided equivalent CO₂ emissions and a payback period of six years.

Keywords: solar desiccant cooling; desiccant wheel (DW); dynamic simulation; thermo-economic analysis; layout modifications

1. Introduction

In the last few years, desiccant and evaporative cooling (DEC) devices have been widely studied as a suitable alternative to conventional electrical-driven heating, ventilation and air conditioning systems (HVAC). They allow several benefits in terms of humidity control, indoor air quality, equivalent CO₂ emissions reduction, primary energy and electricity savings. The last three advantages are further improved considering solar thermal energy as the main source of energy for the plant [1,2].

The solar-driven desiccant and evaporative cooling systems (SDEC) are composed of two main parts: a solar field and an air handling unit (AHU).

In the following literature, special attention is paid to the AHU configurations. Starting from the first system with desiccant wheel (DW) proposed by Pennington [3], other configurations such as recirculation cycle [4], Dunkle cycle [4,5], simplified advanced solid desiccant (SENS) cycle [4,6], revers cycle [4,6], direct-indirect evaporative coolers (DINC) cycle [4,6], and cycles with staged dehumidification/regeneration in one or two rotors [7–10] were introduced.

Some of the newer studies carried out on unconventional DEC-based plants are reported below. In Zhu and Chen [11], a novel marine desiccant-based air conditioning system was developed and studied; experimental tests were performed on a test rig in order to assess the most significant influencing factors on the system efficiency and to find optimal sets of parameters that maximize utilization of the ship residual heat. It was a one-rotor two-stage system with compact size and good performance. The regeneration process was guaranteed by the thermal energy available from the diesel engine and not used for domestic hot water purposes. The cooling process was achieved by direct or indirect contribution of the abundant seawater source.

A two-stage two-rotor system that supplies cool air to produce chilled water was designed, constructed and tested by La et al. [12]. Experimental results obtained under different conditions revealed that the novel device can supply chilled water at 15–20 °C with a thermal coefficient of performance (COP) (ratio between the cooling capacity associated with the cooled water and that for the regeneration) of 0.3–0.6 using a low-grade heat source (solar air collectors). The novel DW-based cooling plant reached a specific thermal COP of about 0.8–0.9 (considering the production of both chilled water and dry air in the ratio with the regeneration power).

Enteria et al. [13,14] considered a SDEC system whose main components were a silica-gel DW, two cross-flow heat exchangers (CFs) and a flat-plate solar subsystem with an electric auxiliary heater. The first measured experimental data showed that about three-quarters of the thermal energy of the system was derived from the solar field and the total COP of the AHU (considering electrical and thermal requests) was 0.25. A more detailed analysis considering different regeneration temperatures (in the range 60–75 °C) showed an improvement of dehumidification performance with the regeneration temperature but a decrease of thermal COP.

Hürdoğan et al. [15] described a new rotary desiccant cooling system with a rotary heat exchanger that is not conventionally used in the DEC plant. It allowed pre-heating of the regeneration air with the exhaust regeneration air. Two other CFs were considered, respectively, for pre-heating of the same regeneration air and for pre-cooling of the process air. Moreover, the system was coupled with an electric chiller to cool down the process air and with an electric heater to heat up the regeneration air. The initial recorded experimental data indicated that in this configuration only 15% of all the energy of cooling is provided by the electric chiller, and only 65% of the regeneration energy is required for regeneration by the electric heat source.

Chung and Lee [16] analyzed the effect of eleven design parameters for two configurations of AHU equipped with DW: in the first case, the pre-heating of the regeneration air was provided by the dehumidified process air; in the second case, the regeneration air was pre-heated with the same exhaust regeneration air. The cooling performance of the regenerative evaporative cooler (EC) was revealed to be the most crucial parameter in the applications of the desiccant-based AHUs with solar systems.

Dynamic simulations were performed by Enteria et al. [17] to compare the operation of a SDEC plant equipped with two coating hygroscopic materials for the DW (silica-gel, titanium dioxide) in three different locations of East Asia. Titanium dioxide revealed higher performance than silica-gel; it achieved lower indoor temperature and humidity ratio.

Zang [18] studied a DW-based AHU with a cooling coil (CC), an enthalpy and a DW. The aim of the work is to determine the optimal values of the control variables in order to minimize the energy consumption satisfying internal thermal comfort criteria. Significant reduction of energy consumption was achieved with the proposed optimized control strategy. Energy savings in the range 27.85%–41.33% were estimated in the different climatic conditions considered.

Ghali [19] analyzed a desiccant-based hybrid air conditioning system in which an electric heat pump (EHP) is integrated in the AHU; the evaporator of the EHP was used to cool the process air while its condenser was used to partially heat the regeneration air. The plant was dimensioned to serve a 150 m² office as replacement of a conventional HVAC system with a 23 kW EHP. In the very humid climatic condition of Beirut (Lebanon), even if the latent load is high, the performance improves.

In fact, a smaller EHP was employed (15 kW), and over 20 years, which is considered a useful life span, economic benefits were obtained.

In the study of Sheng et al. [20], the performance of a DW used in an AHU operating with an integrated high temperature heat pump was evaluated by means of experimental investigation and regression analysis. The combined influences of multiple variables on the performance of the DW, the most influential being regeneration temperature and outdoor air humidity ratio rather than outdoor air temperature and ratio between regeneration and process air flow rates, were investigated based on evaluating different indices such as: dehumidification effectiveness and COP, moisture removal capacity and sensible energy ratio.

Elzahzby et al. [21] predicted through a mathematical model the performance of a solar energy-assisted hybrid AHU with a six-stage one-rotor DW, in which a two-stage dehumidification process, two-stage pre-cooling process and two-stage regeneration process were realized. The authors assessed the influence of operating parameters (rotational speed, process air inlet temperature, humidity ratio and velocity) on some performance indicators (moisture removal capacity, relative moisture removal capacity, dehumidification COP, thermal COP, supply air temperature and humidity ratio), and also discussed the life cycle cost analysis. A payback period of 4.86 years was obtained.

Based on the works described, hereinafter the authors introduce some feasible simple modifications to the hybrid desiccant cooling systems installed at the University of Sannio [22] and then simulated these AHUs coupled with solar collectors (SC) (flat-plate and evacuated tube).

Through TRNSYS (TRaNsient System Simulation program, Solar Energy Laboratory: University of Wisconsin-Madison, Madison, WI, USA) dynamic simulations, the different configurations are evaluated by a thermo-economic assessment and parametric analysis (collector type, surface and tilt angle) are carried out, considering as user a university classroom. The above-described changes are studied to upgrade the existing system installed in the laboratory. These are not all the possible solutions but those that are considered by the scientific literature to have an experimental system standard configuration that can improve system performance with changes that are not too expensive and can be implemented easily.

To the best of the authors' knowledge, although there are numerous papers in the scientific literature analyzing alternative layouts for the desiccant-based AHUs, including those reported in the above literature review, there are only very few studies on the optimal configuration of the solar subsystem for different desiccant HVAC system layouts that consider energy, environmental and economic aspects on an annual basis.

2. Overall Standard Innovative System Description (Scenario A)

2.1. Load Description

A rectangular plan building (63.5 m², 30 seats), located in Benevento (Latitude: 41°08' N; Longitude: 14°47' E) and used as a university classroom, is simulated to determine the sensible and latent loads (Table 1), that are balanced by the desiccant-based and conventional plants compared in this work.

The air conditioning systems are switched on before the building is occupied in order to ensure comfort conditions (20 °C in heating period, 26 °C in cooling period, relative humidity of 50% in both periods) from the outset of the room occupancy, and for the whole opening period (9:00–18:00). A dead band of ±0.5° and ±10% is assumed in the control strategy respectively for temperature and humidity. The main building envelope characteristics are listed in Table 2 [23].

Table 1. Building gains and loads.

Gains Per Occupants (Seated—Very Light Writing, ISO 7730 [24])			
Sensible (W)	65		
Latent (W)	55		
Gain from Artificial Lighting (9:00–18:00) [25]			
Sensible (W/m ²)	10		
Load	Cooling Period	Heating Period	Intermediate Period
Sensible (MWh)	1.54	2.90	-
Latent (MWh)	0.69	0.56	-
Electric (MWh)	0.44	0.56	0.50

Table 2. Building characteristics.

Parameter	Opaque Components				Transparent Components		
	Roof	External Walls (N/S)	External Walls (E/W)	On the Ground Floor	North	South	East/West
U (W/m ² K)	2.30	1.11	1.11	0.297	2.83	2.83	2.83
Area (m ²)	63.5	36	15.87	63.5	8.53	9.40	0.976
g	-	-	-	-	0.755	0.755	0.755

2.2. Innovative Desiccant Air Handling Unit-Based Air Conditioning System

The innovative plant in the standard configuration, for the cooling operation mode, consists of a three-channel AHU equipped with a silica gel DW and a solar subsystem (Figure 1). The HVAC system is arranged on the base of the experimental AHU of University of Sannio (Benevento, Southern Italy). The DW interacts with two air flows: the process air and the regeneration air.

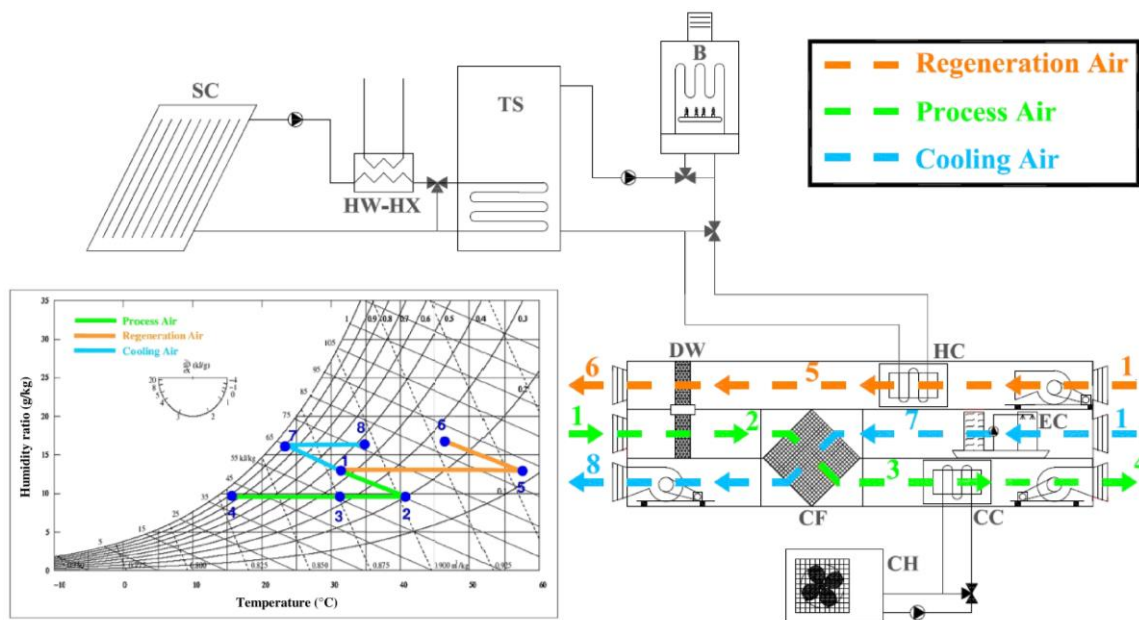


Figure 1. Scheme of the desiccant-based air handling unit (AHU) and psychrometric diagram (cooling mode, Scenario A).

Dehumidification through DW is an exothermic process based on adsorption. While passing through the hygroscopic material, the process air loses some of its vapour content, which is captured by the wheel, and simultaneously heats up (1–2). The moisture content reduction that takes place in this way is managed (through the regeneration air temperature) to completely meet the latent load of the building. This air flow has to be cooled before it is introduced into the room. The cooling process is carried out through an air-to-air CF, (2–3) and a CC, (3–4). In the first heat exchanger, the cooling air flows and heats up (7–8); it is outdoor air cooled by the evaporation of water (1–7) in the EC. The second heat exchanger is fed with cold water from the air-cooled electric chiller, CH. For the application considered in this work, the cooling process is due to the CF for about 1/3 (1.5 MWh/year) and for the remaining 2/3 (2.86 MWh/year) to the CC. In the regeneration section, the DW is deprived of the vapour, that was removed from the process air thanks to a hot air flow (5–6), creating the regeneration air. It is outdoor air heated (1–5) in an air-to-water heat exchanger (HC) fed by the solar subsystem. The SC are assisted by the natural gas boiler (B), which operates as a back-up system when there is an insufficient irradiation level, and heats the water to a temperature that ensures the regeneration of the DW. A thermal storage (TS) tank is used to compensate the uncertainty of the solar source and improve its exploitation by storing the available solar thermal energy during periods of low or zero demand.

During the non-operation periods of the air conditioning plant and whenever the temperature of the fluid (a water/glycol mixture) in the solar loop becomes too high (higher than 100 °C), a cooling system (hot water heat exchanger, HW-HX) operates to produce hot water at 45 °C. Therefore thermal energy obtained from solar energy surplus can be used as domestic hot water, or for low temperature on-site heating processes or by a nearby user with thermal energy requirements, such as a university campus, a gym, a swimming pool, etc.

In the heating mode operation (Figure 2), the regeneration duct, the DW and the electric chiller are excluded, and a post-heating coil (HC2) and a humidifier (EC) are added to the process air duct. In addition, the CC becomes a heating coil (HC) and it is fed by the solar subsystem, no longer by the electric chiller. The AHU consists of a heat recovery process (1–2, 1–6) from the exhaust air of the air conditioned space in the CF, followed by pre-heating (2–3), humidification (3–4) and post-heating (4–5) sections. The solar subsystem with the back-up boiler regulates the water temperature from the TS in order to ensure the necessary heat addition to the two coils, HC and HC2.

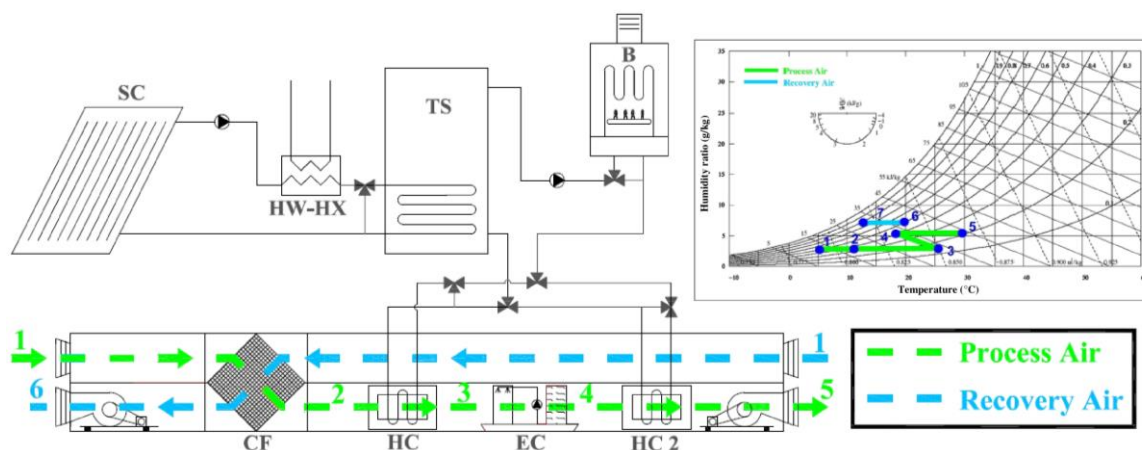


Figure 2. Scheme of the desiccant-based AHU and psychrometric diagram (heating mode, Scenarios A, B, C and D).

The main components of the air conditioning system are previously described by Calise et al. [23] and by Angrisani et al. [22], and detailed information about their characteristics and design condition are reported there.

3. Alternative System Layouts

Starting from the standard configuration of the innovative system (Figure 1, Scenario A), three alternative solutions for the cooling operation are proposed and described below. The DW considered in these three scenarios is the same as the existing experimental plant (Scenario A). Moreover, its rotational speed, the process and regeneration air flowrate, humidity and temperature are fixed (according to the load), so also the DW capacity does not change. Instead, the heating layout remains the same in all scenarios. They are plant modifications related to the AHU to improve system performance. The first alternative Scenario B consists in the recovery of the heat rejected by the condenser of the chiller to pre-heat the regeneration air flow. The second Scenario C consists in the pre-heating of regeneration air with the warmer regeneration air exiting the DW. The last Scenario D involves the pre-cooling of the process air before entering the DW.

These alternative layouts allow to maintain comfort conditions in the conditioned space.

With regards to the solar subsystem, several arrangements differentiated by collector type (flat-plate and evacuated tubes), collecting surface (20, 27 and 34 m²) and tilt angle (20°–55°) are considered. These arrangements are then combined with the three alternative scenarios previously introduced.

The AHU technical and operational details will be illustrated in the following subsections.

3.1. Desiccant-Based Air Handling Unit with Heat Recovery from Chiller Condenser (Scenario B)

In hybrid desiccant-based plants, it is convenient to use integrated heat pump systems: cooling energy from the chiller (evaporator) is used for an accurate control of the supply air temperature, and thermal energy (condenser) is used to pre-heat the regeneration air flow.

In the standard configuration (Scenario A, Figure 1), the chiller supplies cooling energy only, to control the temperature of the process air. Thermal energy of the condensation phase (rejected heat) is dissipated in the environment. Therefore, a first modification to the standard plant consists in recovering part of the condensation heat by using a share of the condenser air flow rate (3300 m³/h) as regeneration air.

As regards the process and cooling air flows, the AHU (Figure 3) remains unchanged compared to the standard configuration, whereas for the regeneration air (psychrometric diagram, Figure 3), a pre-heating process with heat recovery from chiller condenser appears (1–5), thereby reducing the contribution from the HC (5–6) that is used to ensure the required temperature for the regeneration process (6–7).

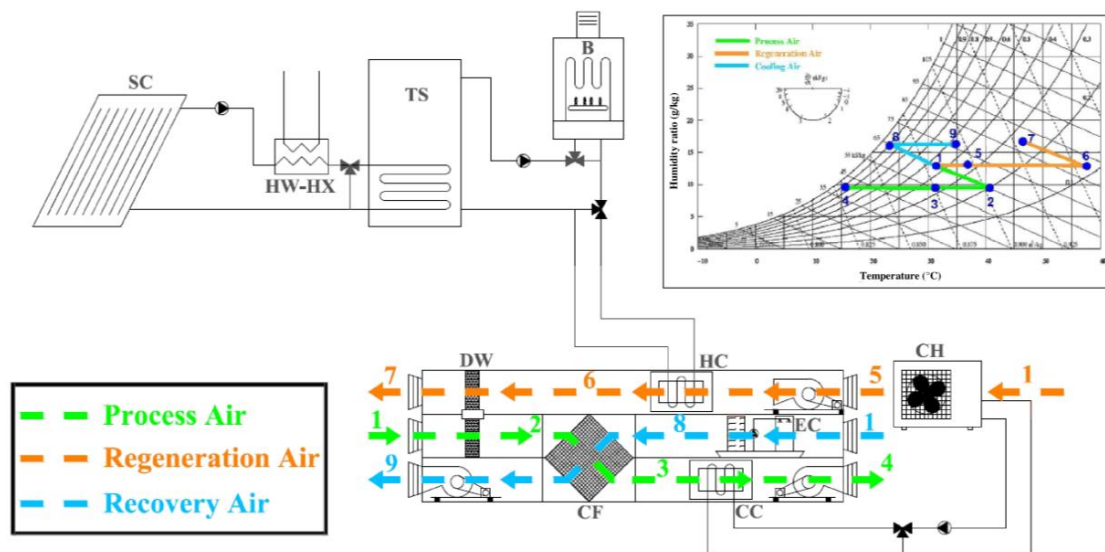


Figure 3. Scheme of the desiccant-based AHU with heat recovery from chiller condenser and psychrometric diagram (cooling operation, Scenario B).

3.2. Desiccant-Based Air Handling Unit with Cross-Flow Heat Recovery Unit (Scenario C)

In the hybrid AHU, the highest temperature level is reached by the regeneration air before passing through the DW; at the outlet of this component, the air still has a temperature greater than the outside one. It can therefore be advantageously used to pre-heat the regeneration air flow drawn from the outside.

Several devices exist for heat recovery [26]. In this case, a CF, CF2 (Figure 4), is used, and simulated using experimental results for the CF of the test facility (CF) to calibrate and validate the model. Therefore, the regeneration air (psychrometric diagram, Figure 4) is pre-heated (1–5) in CF2, further heated in HC (5–6) with the thermal energy supplied by the solar subsystem, before proceeding to regenerate the DW (6–7) and passing through the recuperative heat exchanger CF2 (7–8). The HC has the task of ensuring the desired regeneration temperature.

Due to the presence of this new component, a higher power requirement for the regeneration fan is assumed (350 W). Also in this scenario, the cooling and process air ducts remain identical to those of the standard plant.

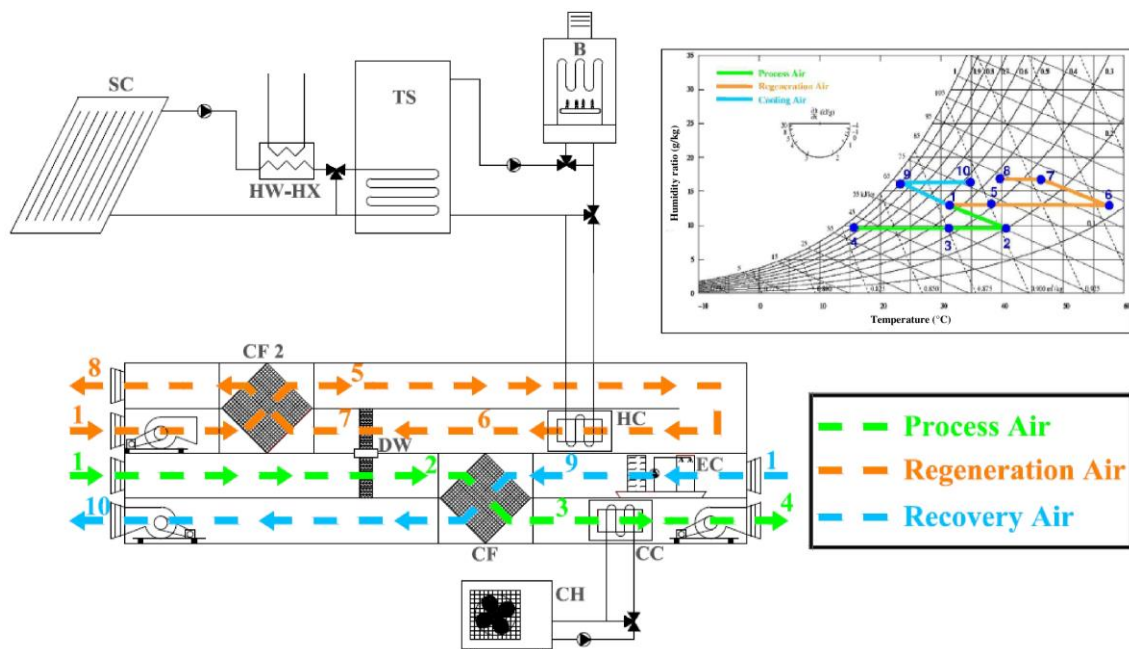


Figure 4. Scheme of the desiccant-based AHU with cross-flow heat recovery unit and psychrometric diagram (cooling operation, Scenario C).

3.3. Desiccant-Based Air Handling Unit with Pre-Cooling of Process Air (Scenario D)

Pre-cooling/dehumidification of the process air before dehumidification with DW has two advantages:

- (1) allows the operation even in places characterized by very humid climates [27];
- (2) reduces the regeneration temperature for a given value of the desired humidity ratio reduction [28].

Analyzing the simulated and experimental results of the standard configuration, one notes that the chilled water temperature after the heat exchange in the CC is still lower than that of the outside air, so the possibility of employing a pre-cooling coil (CC2) (Figure 5) can be evaluated. In some climatic conditions (high relative humidity), a slight pre-dehumidification process can also occur in this CC2.

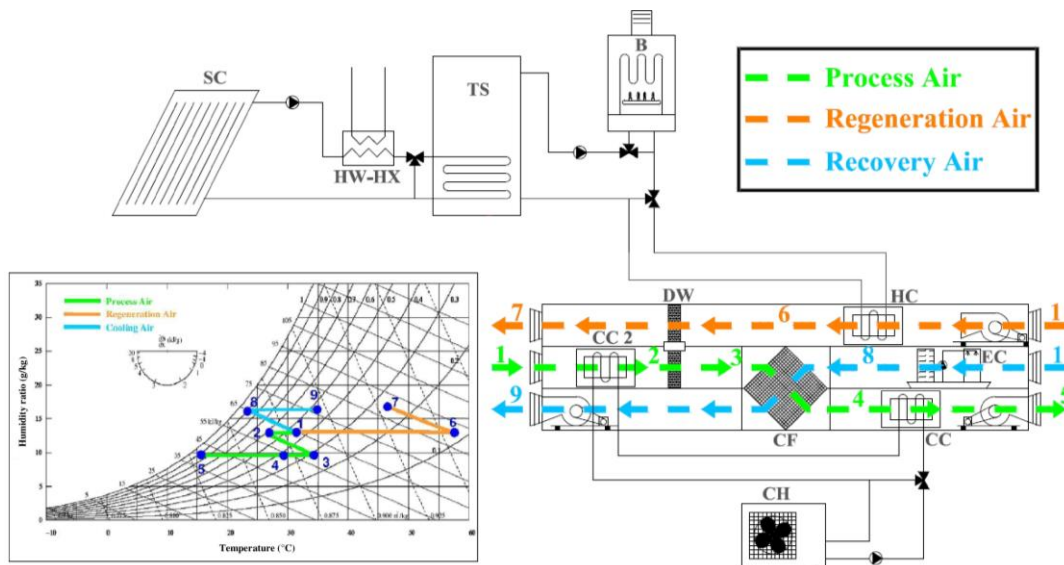


Figure 5. Scheme of the desiccant-based AHU with pre-cooling coil (CC2) and psychrometric diagram (cooling operation, Scenario D).

In this scenario, the transformations (psychrometric diagram, Figure 5) of the regeneration and cooling air remain unchanged with respect to standard configuration; instead, the process air is firstly pre-cooled (1–2), then dehumidified by adsorption (2–3), cooled in CF (3–4), and finally cooled in CC (4–5).

4. Conventional System Layout

A standard AHU with cooling dehumidification (1-A) and post-heating (A-4) constitutes the simulated air conditioning system in the conventional system (CS) during cooling period (Figure 6). A vapor compression chiller with a cooling capacity of 16 kW feeds the cooling and dehumidification coil, whereas a 24 kW boiler ($\eta_B = 90.2\%$) feeds the post-HC [1,29]. This boiler has the same characteristics of that in the AS. In the heating period, the simulated AHU of the CS is the same of the AS (Figure 2), but the HCs are fed by the natural gas boiler only. All electricity of the conventional HVAC system is taken from the grid and hot water is produced with the boiler.

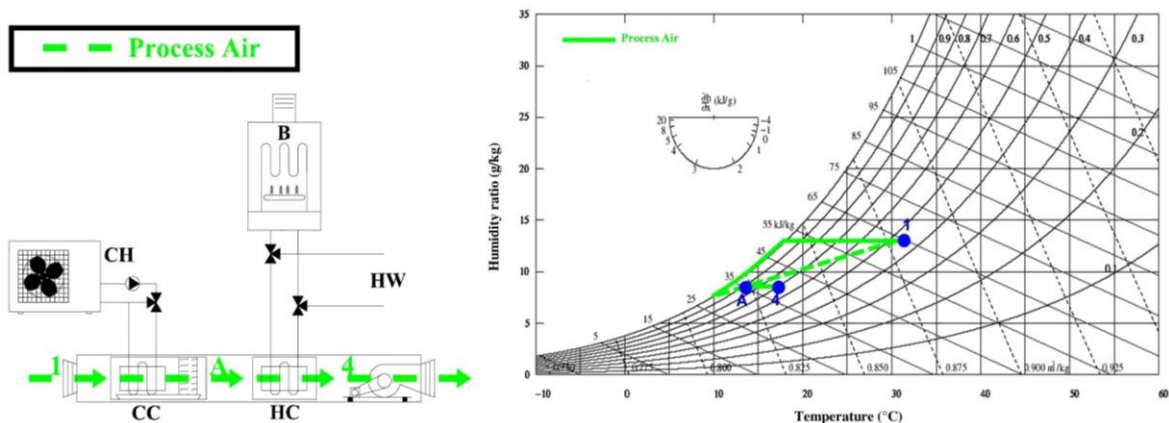


Figure 6. Scheme of the standard AHU and psychrometric diagram.

5. Model and Performance Assessment Methodology

Dynamic simulations with a time step of 1.5 min have been carried out using the software “TRNSYS 17” [30] integrated with the “TESS” (Thermal Energy Systems Specialists, Madison, WI, USA) libraries [31]. The models of the main plant components were described and characterized in detail in previous works [1,32,33].

The component parameters have been chosen on the basis of experimental values, when available, or otherwise according to the rated values.

Therefore, only some details of the main components are presented below:

- SC: the model is based on the following expression for the efficiency [34]:

$$\eta_{\text{col}} = \eta_0 - a_1 \frac{\Delta T}{G} - a_2 \frac{\Delta T^2}{G} \quad (1)$$

where the temperature differences characterize the thermal energy losses between the heat transfer fluid and the outdoor environment and the constant term represents the optical performance. This last term is corrected according to the incident angle modifier (IAM). It is a second-order polynomial (function of the incident angle with the constant equal to 1) for the flat-plate collectors and the product of transversal and longitudinal IAM factors (they are typically proposed by manufactures in tables or figures) for the evacuated tube collectors.

- DW: the two efficiencies, η_{F1} and η_{F2} , calculated with the potentials F_1 and F_2 , are used [35]:

$$\eta_{F1} = (F_{1,2} - F_{1,1}) / (F_{1,5} - F_{1,1}) \quad (2)$$

$$\eta_{F2} = (F_{2,2} - F_{2,1}) / (F_{2,5} - F_{2,1}) \quad (3)$$

$$F_{1,j} = \frac{-2865}{(t_j + 273.15)^{1.49}} + 4.344 (\omega_j / 1000)^{0.8624} \quad (4)$$

$$F_{2,j} = \frac{(t_j + 273.15)^{1.49}}{6360} - 1.127 (\omega_j / 1000)^{0.07969} \quad (5)$$

where the subscript “ j ” refers to the generic air state at which the two potentials are evaluated, whereas t and ω are the air temperature ($^{\circ}\text{C}$) and the humidity ratio (g/kg), respectively.

These two potentials allow to assimilate the complex phenomenon (adsorption), that takes place in the DW, to the simple heat transfer process in a heat exchanger. The model has been validated and calibrated with experimental data [32].

- Storage tank: the model simulates the tank as a cylinder divided in a series of superimposed sections (called “nodes”) at uniform temperature. Each node thermally interacts with the upper and the lower nodes, with the outdoor environment, with internal heat exchangers and with two water flowrates entering/leaving the tank from/to the outside. The energy balance for a node is:

$$\begin{aligned} (m_i C_p) \frac{dT_i}{d\tau} = & \frac{(k+\Delta k)A_{c,i}}{\Delta x_{i+1 \rightarrow i}} (T_{i+1} - T_i) + \frac{(k+\Delta k)A_{c,i}}{\Delta x_{i-1 \rightarrow i}} (T_{i-1} - T_i) + (U_{\text{tank}} + \Delta U_i) A_{s,i} (T_a - T_i) + \dot{m}_{\text{down}} C_p T_{i-1} \\ & - \dot{m}_{\text{up}} C_p T_i - \dot{m}_{\text{down}} C_p T_i - \dot{m}_{\text{up}} C_p T_{i+1} + UA_{\text{hx}1} \Delta T_{\text{In}1} + UA_{\text{hx}2} \Delta T_{\text{In}2} + UA_{\text{hx}3} \Delta T_{\text{In}3} + \dot{m}_{1\text{in}} C_p T_{1\text{in}} - \dot{m}_{1\text{out}} C_p T_i \\ & + \dot{m}_{2\text{in}} C_p T_{2\text{in}} - \dot{m}_{2\text{out}} C_p T_i \end{aligned} \quad (6)$$

where the term on the left side represents the time variation of energy in the node, the first two terms on the right side represent the conductive interactions with the upper and lower one; the third term evaluates the heat losses towards the surrounding ambient; the terms related to \dot{m}_{up} , \dot{m}_{down} , \dot{m}_{in} and \dot{m}_{out} are the convective terms, and the remaining terms, marked with the subscript “hx,” represent the contributions of the exchangers.

This model has been validated and calibrated with experimental data in [33].

The most important parameters of the components described above and of the other main plant devices, their TRNSYS types and references in which their validation processes were carried out, are listed in the following Tables 3 and 4.

Table 3. Main models used for the simulation and their main parameters. DW: desiccant wheel; TESS: Thermal Energy Systems Specialists; CF: cross-flow heat exchanger; COP: coefficient of performance; HC: heating coil; CC: cooling coil; SC: solar collector; IAM: incident angle modifier.

Component (Reference)	Type	Library	Main Parameters	Values	Units
Building	56	Standard	See Tables 1 and 2		
DW [32]	1716	TESS	Effectiveness η_{F1} Effectiveness η_{F2}	0.207 0.717	- -
CF [32]	91	Standard	Effectiveness	0.446	-
Humidifier [32]	506c	TESS	Saturation efficiency	0.551	-
Natural gas boiler [32]	6	Standard	Nominal thermal power Efficiency	24.1 0.902	kW -
Air-cooled chiller [32]	655	TESS	Rated capacity Rated COP	8.50 2.98	kW -
HC [32]	670	TESS	Liquid-specific heat Effectiveness	4.190 0.864	$\text{kJ}/(\text{kg}\cdot\text{K})$ -
CC [32]	508	TESS	Liquid-specific heat Bypass fraction	4.190 0.177	$\text{kJ}/(\text{kg}\cdot\text{K})$ -
Flat-plate SC	1b	Standard	Tested flow rate	0.0112	$\text{kg}/(\text{s}\cdot\text{m}^2)$
			Intercept efficiency η_0	0.673	-
			Efficiency slope a_1	2.98	$\text{W}/(\text{m}^2\cdot\text{K})$
			Efficiency curvature a_2	0.0078	$\text{W}/(\text{m}^2\cdot\text{K}^2)$
			Fluid-specific heat	3.84	$\text{kJ}/(\text{kg}\cdot\text{K})$
			First-order Incident Angle Modifier coefficient	0.072	-
			Second-order Incident Angle Modifier coefficient	0.00	-
Storage tank [33]	60f	Standard	Volume	971	l
			Height	2.04	m
			Tank loss coefficient	1.37	$\text{W}/(\text{m}^2\cdot\text{K})$
			Liquid-specific heat	4.190	$\text{kJ}/(\text{kg}\cdot\text{K})$
Evacuated SC	71	Standard	Tested flow rate	$8.43\cdot 10^{-3}$	$\text{kg}/(\text{s}\cdot\text{m}^2)$
			Intercept efficiency η_0	0.676	-
			Efficiency slope a_1	1.15	$\text{W}/(\text{m}^2\cdot\text{K})$
			Efficiency curvature a_2	0.004	$\text{W}/(\text{m}^2\cdot\text{K}^2)$
			Fluid-specific heat	3.85	$\text{kJ}/(\text{kg}\cdot\text{K})$
			IAM data	See Table 4	

Table 4. Evacuated tube collectors IAM factors.

Direction (°)	Transversal IAM	Longitudinal IAM
0	1.00	1.00
10	1.00	1.00
20	1.00	1.00
30	1.00	1.00
40	1.03	0.98
50	1.08	0.96
60	1.15	0.87
70	1.11	0.72
80	0.72	0.50
90	0.00	0.00

The performance assessment is realized through the comparison of the alternative systems (AS) and CS on energy, environmental and economic bases. The primary energy and the equivalent CO_2 emissions percent differences between CS and AS, primary energy saving (PES) and equivalent CO_2 avoided emission (ΔCO_2), respectively, have been calculated:

$$PES = \left(1 - E_p^{AS}/E_p^{CS}\right) \times 100 \quad (7)$$

$$\Delta CO_2 = \left(1 - CO_2^{AS}/CO_2^{CS}\right) \times 100 \quad (8)$$

where the primary energy and the equivalent CO₂ emissions of the alternative and CS ($E_p^{AS/CS}$ and $CO_2^{AS/CS}$) are evaluated as:

$$E_p^{AS/CS} = (E_{el,chil}^{AS/CS} + E_{el,aux}^{AS/CS})/\eta_{EG} + E_{th,B}^{AS/CS}/\eta_B \quad (9)$$

$$CO_2^{AS/CS} = \left(E_{el,chil}^{AS/CS} + E_{el,aux}^{AS/CS}\right) \times \alpha + E_{th,B}^{AS/CS} \times \beta/\eta_B \quad (10)$$

In Equations (9) and (10), $E_{el,chil}^{AS/CS}$ represents the electric energy required by the chiller in the AS and CS; $E_{el,aux}^{AS/CS}$ represents the electric energy required by the HVAC auxiliaries for both AS and CS; and $E_{th,B}^{AS/CS}$ the heat supplied by the boiler in AS and CS. Furthermore, the energy efficiency of the Italian national electric system (η_{EG}) and of the boiler (η_B) are assumed equal to 42% [36–38] and 90.2% [29], respectively. The specific emission factor of primary energy due to natural gas combustion, β is equal to 0.207 kgCO₂/kWh_{EP}, [39], and α the specific emission factor of electricity drawn from the grid is equal to 0.573 kgCO₂/kWh_{el}, [29].

The economic analysis is performed by calculating the simple payback period (SPB):

$$SPB = EC / \sum_{k=1}^N F_k \quad (11)$$

where N is the number of years to pay back the investment, EC is the extra cost of the AS (desiccant-based AHU, storage tank and collectors) with respect to the reference system (CS), and F_k is the cash flow for the generic year k :

$$F_k = OC^{CS} - OC_k^{AS} \quad (12)$$

where OC_k^{AS} and OC^{CS} are the operating costs of the AS and CS; the former is calculated as:

$$OC_k^{AS} = \sum_r V_{NG,r} c_{NG,r} + \left(E_{el,chil}^{AS} + E_{el,aux}^{AS}\right) \times c_{el} + MC_B + MC_{chil}^{AS} + MC_{col} - I_{a,tot} \quad (13)$$

where taking into account Italian conditions and components characteristics the following assumptions, were considered:

- lower heating value (LHV) of natural gas equal to 9.52 kWh/Nm³;
- the total volume of natural gas $V_{NG,tot} = \sum_r V_{NG,r} = E_{th,B}/(\eta_B \times LHV)$ should be divided according to the brackets of Table 5, to which different unitary costs ($c_{NG,r}$) are associated;
- unitary cost of electricity (c_{el}) equal to €0.211/kWh;
- extra cost of desiccant-based AHU with respect to the conventional one equal to €10,000, it also includes maintenance costs, as provided by the purchase contracts;
- investment cost of storage tank equal to €3,000;
- investment cost of chiller: €3,000 for the AS and €6,000 for the CS;
- specific cost of collectors (c_{col}) equal to €360/m² and €600/m² for flat-plate and evacuated tube collectors, respectively;
- maintenance cost of the boiler (MC_B) equal to €80/year;
- maintenance cost of the chiller in the AS (MC_{chil}^{AS}) equal to €150/year [29];
- maintenance cost of the SC ($MC_{col} = mc_{col} \times S \times c_{col}$) with specific maintenance cost mc_{col} equal to 2% and S gross SC area [40];

- incentive, provided for two years (the installed surface is lower than 50 m²), it is evaluated as $I_{a,tot} = C \times S$ where $I_{a,tot}$ is the annual economic incentive, with C as a valorization coefficient depending on the type of plant (equal to €255/m² for solar cooling systems).

Table 5. Unitary costs.

r	Volume Brackets (Nm ³)	$c_{NG,r}$ (€/Nm ³)
1	1–120	0.561
2	121–480	0.884
3	481–1560	0.912
4	1561–5000	0.943
5	5001–80,000	0.896

OC^{CS} , instead, was calculated with an equation similar to Equation (13) but without incentive and with a maintenance cost for the chiller MC_{chil}^{AC} equal to €288/year.

6. Results

The operation of the alternative and CSs is simulated considering space-cooling energy demands during weekdays of the summer season (1 June–15 September); space-heating energy demands during weekdays of winter period (15 November–31 March); hot water production for further thermal energy demands (with solar thermal energy surplus) all year long.

The electrical devices of the classroom are turned on during its opening hours (Monday–Friday; 9:00–18:00).

Three subscenarios are also considered: 0%, 50% and 100% of thermal energy of the hot water produced from solar surplus (HW-HX) is effectively used for further demands.

In all configurations it is assumed that the collectors face south, as this orientation is the one that allows consistent obtaining of the maximum PES, regardless of the angle of inclination. As an example, the figure obtained for the standard system with 34 m² of evacuated tube collectors is reported (Figure 7).

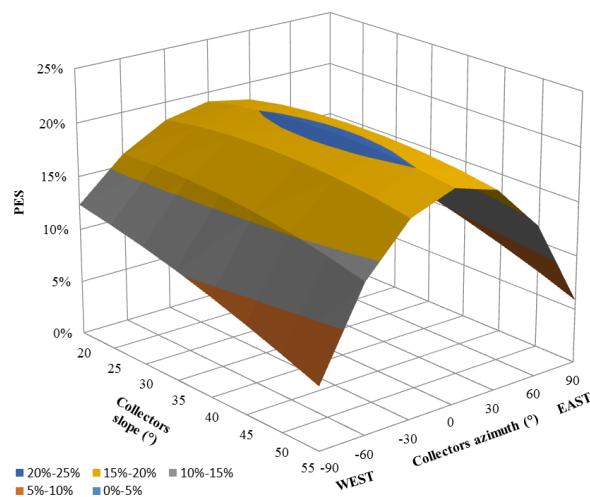


Figure 7. Primary energy saving of the alternative system (AS) (Scenario A) with 0% of solar thermal energy surplus used and evacuated tube collectors as a function of azimuth and tilt angle.

In order to have an immediate view of the advantages deriving from the plant modification, the performance curves of the standard configuration, Scenario A, are shown below. The four graphs, labeled “(a)”, “(b)”, “(c)”, and “(d)” in the following Figures 8–11, show the results of the comparison between the ASs and the conventional one (respectively for Scenarios A, B, C and D).

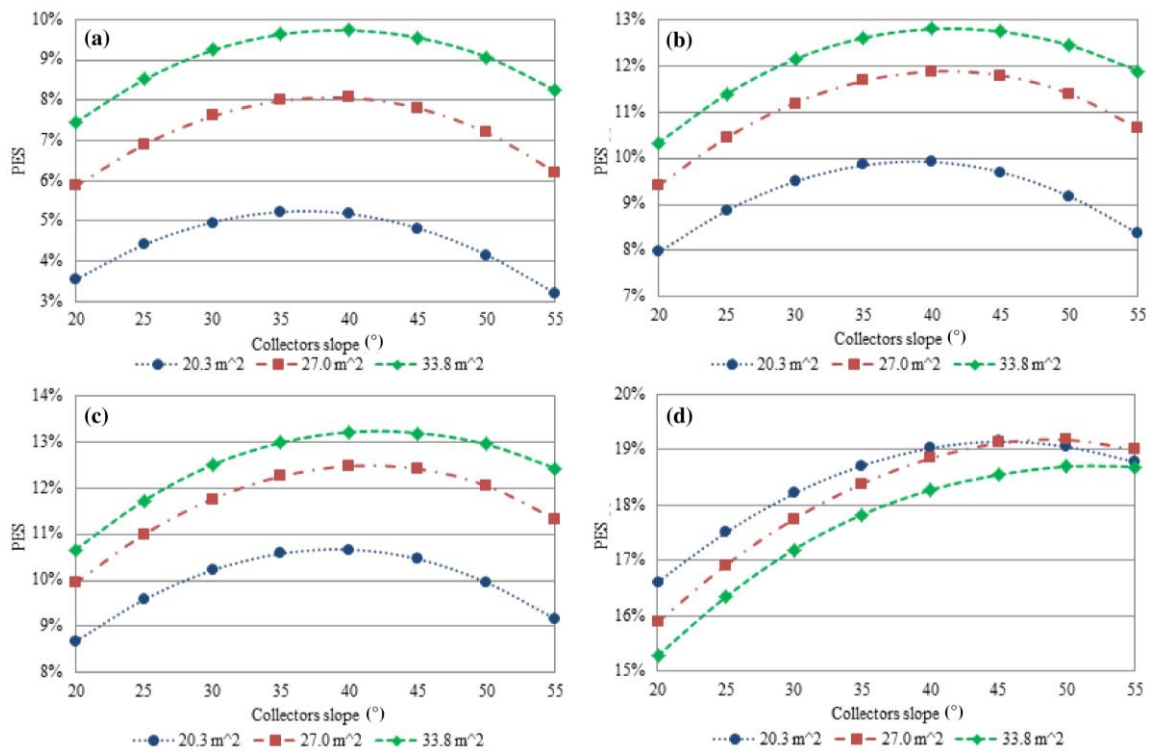


Figure 8. Primary energy saving of the ASs with 0% of solar thermal energy surplus used and flat-plate collectors in the four alternative configurations: (a) Scenario A; (b) Scenario B; (c) Scenario C; and (d) Scenario D.

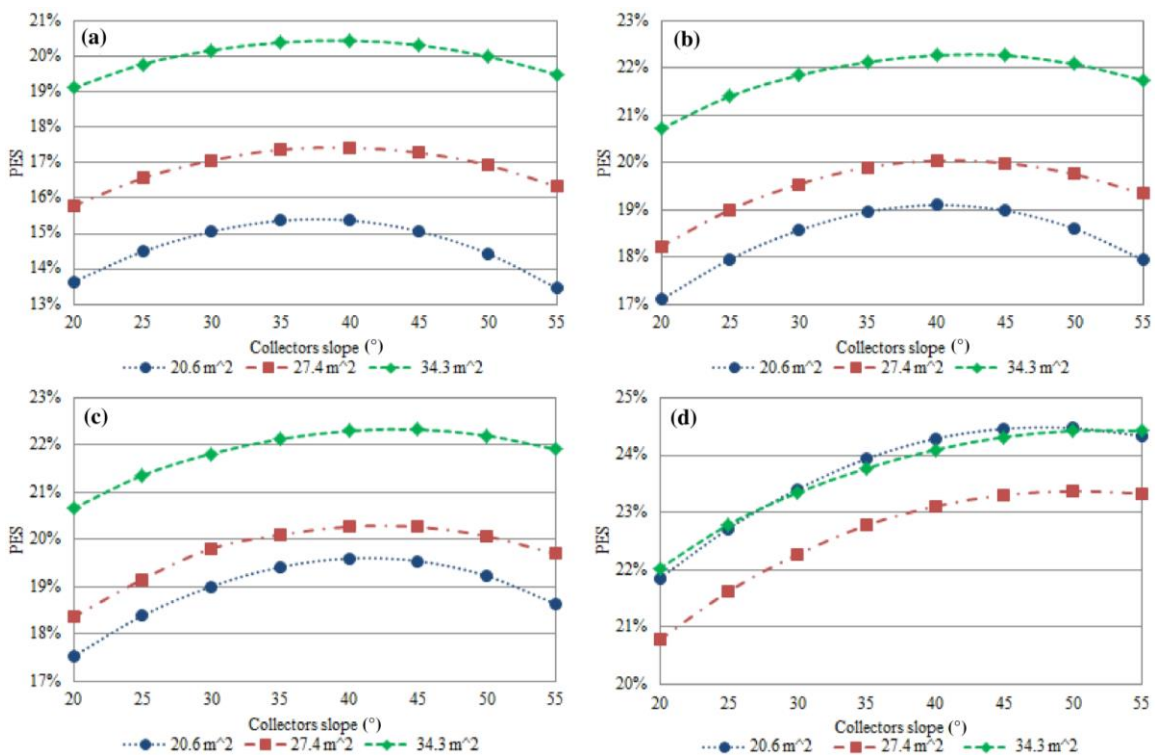


Figure 9. Primary energy saving of the ASs with 0% of solar thermal energy surplus used and evacuated tube collectors in the four alternative configurations: (a) Scenario A; (b) Scenario B; (c) Scenario C; and (d) Scenario D.

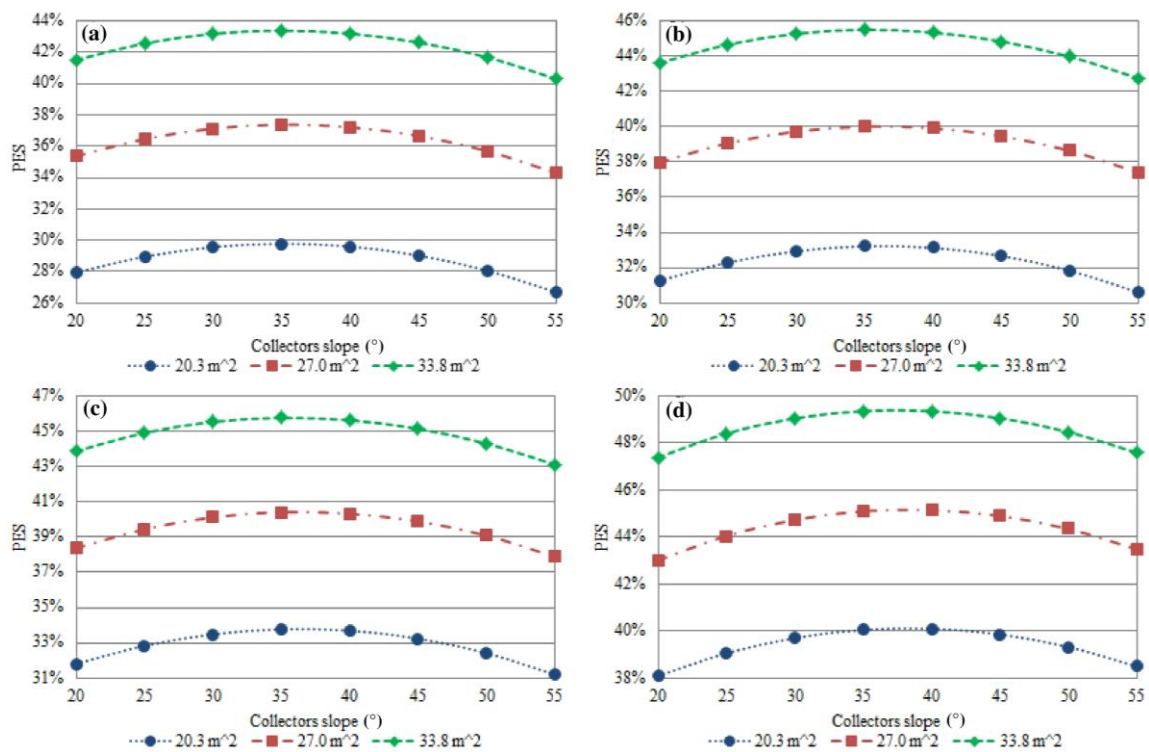


Figure 10. Primary energy saving of the ASs with 50% of solar thermal energy surplus used and flat-plate collectors in the four alternative configurations: (a) Scenario A; (b) Scenario B; (c) Scenario C; and (d) Scenario D.

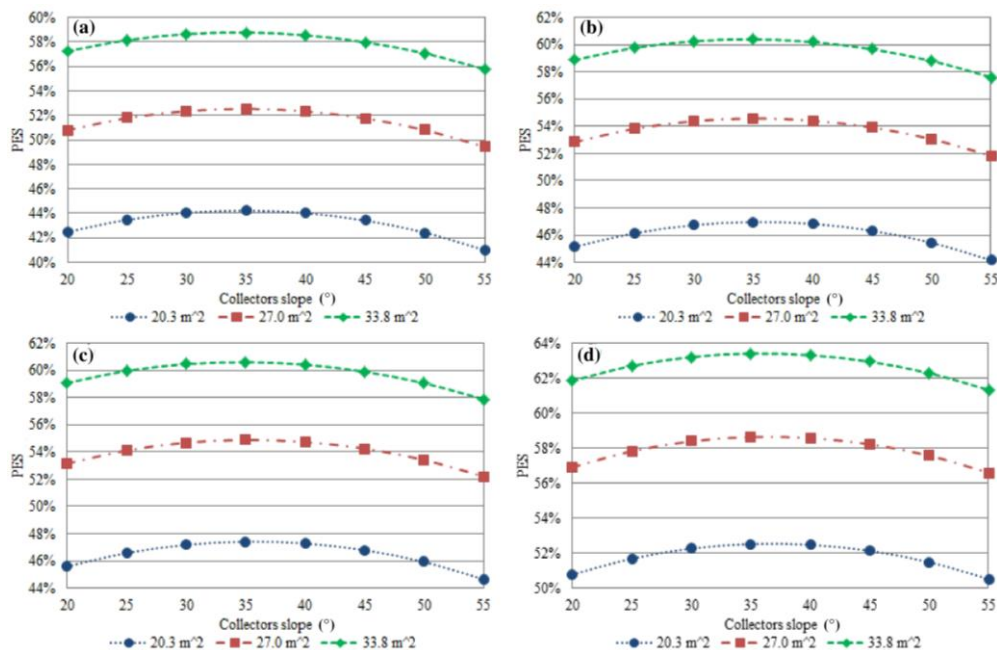


Figure 11. Primary energy saving of the ASs with 100% of solar thermal energy surplus used and flat-plate collectors in the four alternative configurations: (a) Scenario A; (b) Scenario B; (c) Scenario C; and (d) Scenario D.

Regarding the energy analysis, the *PES* index, as a function of the SC slope and area, is reported in Figures 8, 10 and 11 for the hybrid AHU with flat collectors and in Figure 9, and Table 6 for the same AHU with evacuated tube collectors. The results reveal that:

- (1) The *PES* is always positive; therefore ASs are always energetically convenient with respect to CS;
- (2) The energy performance, as expected, improves with increasing collector area except for Scenario D when 0% of solar thermal energy surplus used is considered (Figures 8d and 9d);
- (3) The systems with evacuated tube collectors are generally more efficient than those with flat-plate collectors: there is a difference of about ten percentage points in the standard configuration (Scenario A, Figures 8a and 9a) and in those with the pre-heating process (Scenarios B and C, Figures 8b,c and 9b,c); six percentage points in the system with the CC2 (Scenario D, Figures 8d and 9d);
- (4) Modifications to the AHU when it is coupled to evacuated tube collectors provide lower improvements in the annual operation (Figure 9b,c); in fact, there is an increase of only two to three percentage points in the scenarios that involve pre-heating of the regeneration air (Scenario B and C) compared to the AS without modifications (Scenario A). With flat-plate collectors, the increase is slightly higher, 3%–5% (Figure 8b,c);
- (5) Although the trends of Scenario D and A are not similar, the Scenario D associated with evacuated collectors provides an average smaller percentage of improvements to Scenario A with respect to the same configuration coupled with flat-plate collectors (Figures 8 and 9);
- (6) Scenario D shows some anomalies (they will be better clarified at the following points 13 and 14) when 0% of solar thermal energy surplus use is considered (Figures 8d and 9d). It allows getting the best performance but it is also the least affected by the increase of the collector area, confirming the fact that with the process air pre-cooling, less energy is required to regenerate the DW;
- (7) Scenario B and C with 0% of solar thermal energy surplus used show similar performance, although the second one is slightly more effective (Figures 8 and 9b,c);
- (8) With 0% of solar thermal energy surplus used and flat-plate collectors, the maximum *PES* is obtained for a tilt angle of 40°, except in Scenario D (Figure 8), while with evacuated tube collectors, the optimum tilt angle is 40°–45° (Figure 9);
- (9) For Scenario D with 0% of solar thermal energy surplus used (Figures 8d and 9d) the maximum *PES* occurs at tilt angles of 45°–55° as the energy benefits are especially derived from the winter exploitation of solar energy when the sun is lower on the horizon, while the regeneration energy is significantly reduced;
- (10) If a certain amount of solar thermal energy surplus is used, a homogenization of *PES* curves appears and for all the analyzed solutions the optimal tilt angle is 35° (Figures 10 and 11 and Table 6). Figures 10 and 11 show the *PES* trends in the case of systems with flat-plate collectors when solar thermal energy surplus are exploited for half or total, respectively. Conversely, for the layouts with evacuated tube collectors, only the maximum values are reported in Table 6; the trends remain the same for solutions with flat-plate collectors only shifted upwards. Because of the long periods (intermediate season and weekends) in which the AHU is off and the solar energy is not exploited for air conditioning, the amount of energy associated with the solar surplus becomes preponderant with respect to the other thermal energy flows;
- (11) Even if only 50% of the solar thermal energy surplus is used, a huge performance improvement appears; the best solution (34 m² of collectors and CC2, Scenario D) ensures a *PES* of about 50% with flat-plate collectors (Figure 10d), that grows over 61% with evacuated tube collectors (Table 6);
- (12) Taking into account 100% use of solar thermal energy surplus, the maximum *PES* always occurs in Scenario D, with a tilt angle of 35° and the maximum SC area (34.3 m²). The performance increases to a *PES* of over 63% (Figure 11d) and about 74% (Table 6) for flat-plate and evacuated tube collectors, respectively;

- (13) In Scenario D, with flat-plate collectors and tilt angles up to 45° (Figure 8d), the system is more efficient with lower absorbing surfaces. This situation arises from the fact that with 0% of solar thermal energy surplus used, the annual increase in electricity demand ($E_{p,el,WD,Su}$; $E_{p,el,WD,Wi}$; $E_{p,el,Int}$; $E_{p,el,WED}$ in terms of primary energy), due to the operation of the solar loop, is not accompanied by a sufficient reduction of the thermal energy ($E_{p,th,WD,Su}$ in terms of primary energy) required by the AHU in the summer (Figure 12). In fact, the summer solar fraction (the percentage of thermal energy for regeneration supplied by the solar subsystem) is very high, about 85%, even with 20 m² of collectors.
- (14) Scenario D with 27 m² of evacuated tube collectors shows the worst performance (Figures 9d and 13) among the investigated surfaces. The curves for 20 m² and 34 m² almost overlap, as moving from the former to the latter, the increase in electricity demand of the solar subsystem balances the increased availability of thermal energy on an annual basis. The summer solar fraction is greater than 94% with 20 m² of collectors.

Table 6. Best PES with evacuated tube collectors and solar thermal energy recovery of 50% and 100%.

Evacuated Tube Collectors	Scenario A		Scenario B		Scenario C		Scenario D	
Surface (m ²)	50%	100%	50%	100%	50%	100%	50%	100%
20.6	43.15	57.17	45.83	59.32	46.19	59.61	50.02	62.78
27.4	51.04	65.18	52.93	66.67	53.13	66.84	55.50	68.74
34.3	58.15	71.60	59.44	72.58	59.52	72.65	61.05	73.84

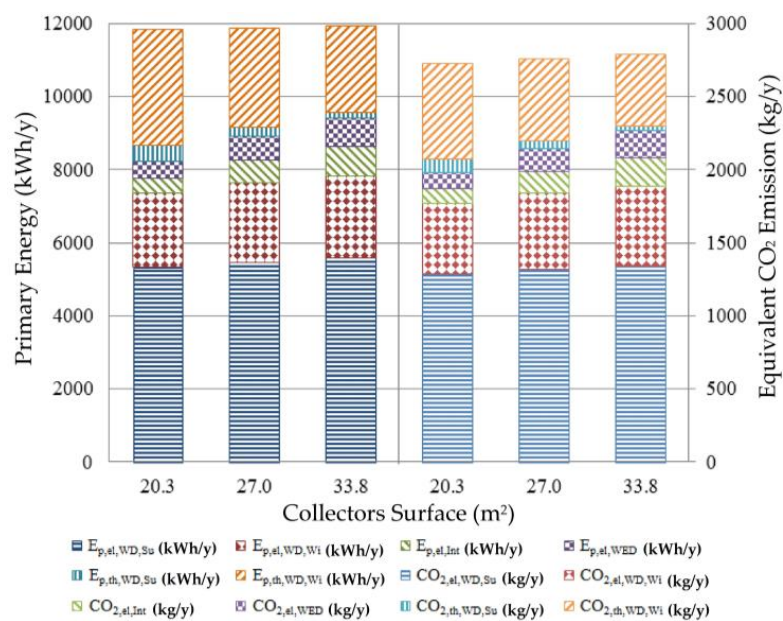


Figure 12. Annual primary energy consumption and equivalent CO₂ emission for the plant with pre-CC (Scenario D), flat-plate collectors, 40° tilt angle and 0% of solar thermal energy surplus used.

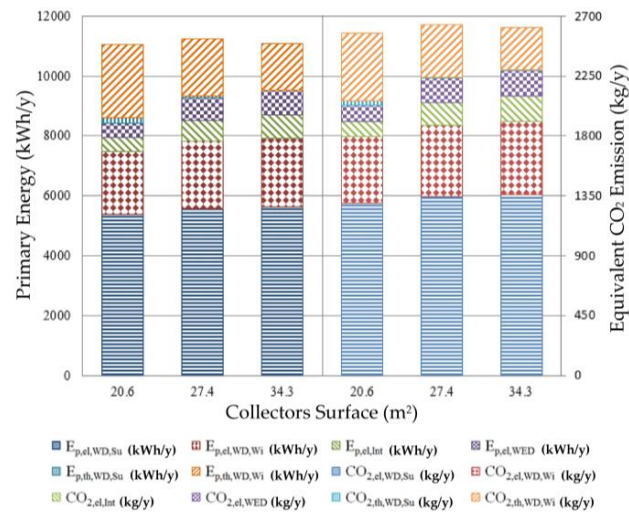


Figure 13. Annual primary energy and equivalent CO₂ emission associated with seasonal electric and thermal demands for the plant with CC2 (Scenario D), evacuated tube collector, 40° tilt angle and 0% of solar thermal energy surplus used.

With regard to the equivalent CO₂ emissions, the results are in part different from the energetic ones. In particular:

- (1) Scenario D with flat-plate collectors always operates better with smaller absorbing surfaces (Figure 14d);
- (2) Scenario D with evacuated tube collectors (Figure 15d) and an absorbing surface of 27 m² has higher emissions; it is better with 34 m² and even better with 20 m²;
- (3) Scenarios B and C with flat-plate collectors (Figure 15b,c) show that, by increasing the absorbing surface from 27 m² to 34 m², emissions benefits decrease with respect to the increase from 20 m² to 27 m². On the contrary, the environmental performance of systems with 20 m² and 27 m² of evacuated tube collectors are very similar (Figure 15b,c).

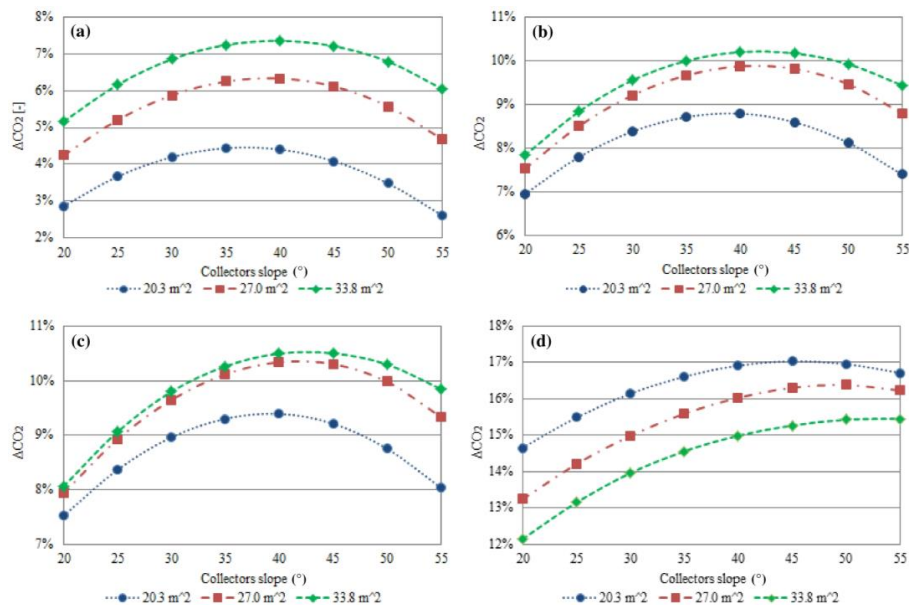


Figure 14. Equivalent CO₂ avoided emissions of the ASs with 0% of solar thermal energy surplus used and with flat-plate collectors in the four alternative configurations: (a) Scenario A; (b) Scenario B; (c) Scenario C; and (d) Scenario D.

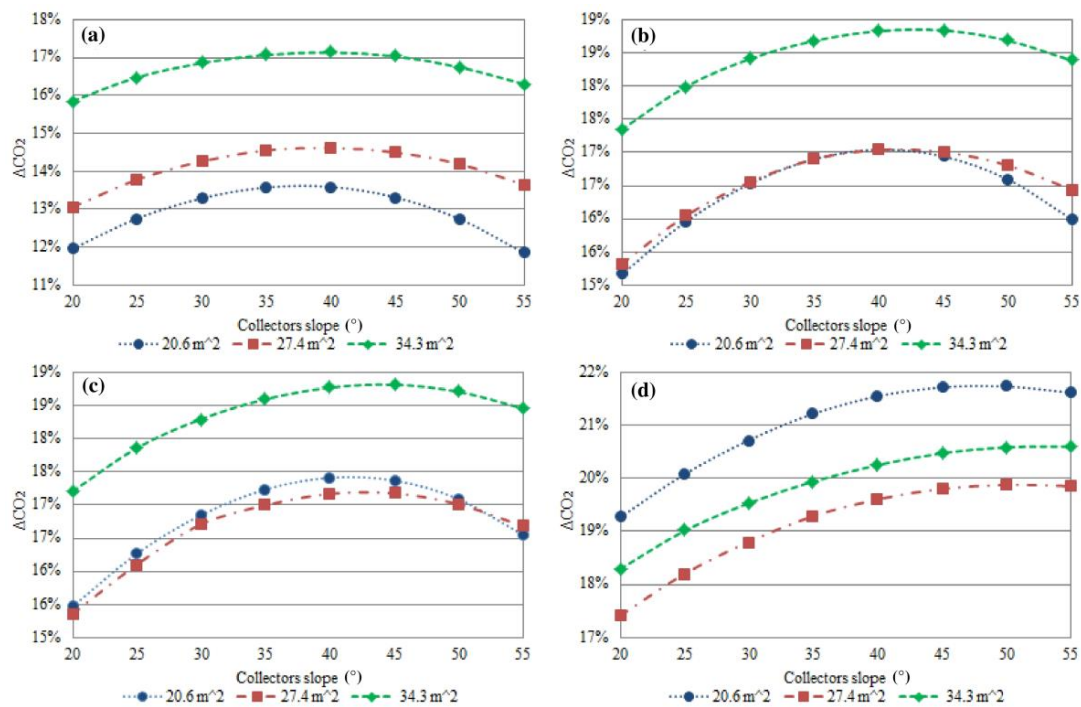


Figure 15. Equivalent CO₂ avoided emissions of the ASs with 0% of solar thermal energy surplus used and with evacuated tube collectors in the four alternative configurations: (a) Scenario A; (b) Scenario B; (c) Scenario C; and (d) Scenario D.

For the sake of brevity, the curves of the avoided equivalent CO₂ emissions in the case of total and partial (50%) use of solar thermal energy surplus are not shown. Their trends, as a function of the tilt angle and of the collectors surface, are similar to those of *PES*.

In order to find the energy demands that mainly affect energy and environmental performance, in Figures 12, 13 and 16, the share of primary energy consumption and CO₂ emission are shown. The subscripts el and th indicate the primary energy associated, respectively, with the electrical and thermal demands of the plant. It can be observed that:

- (1) the primary energy and the equivalent CO₂ emission associated with the summer electrical requirements for all systems ($E_{p,el,WD,Su}$ and $CO_{2,el,WD,Su}$) are always the largest amounts and increase with the collecting surface;
- (2) the primary energy and the equivalent CO₂ emission associated with the electrical requirements of the periods when the air conditioning is turned off ($E_{p,el,Int}$; $E_{p,el,WED}$ and $CO_{2,el,Int}$; $CO_{2,el,WED}$) increase with the collector area, but they are less important than the other electrical loads;
- (3) the primary energy demand of the boiler in winter ($E_{p,th,WD,Wi}$) is higher than in summer ($E_{p,th,WD,Sum}$);
- (4) the primary energy and the equivalent CO₂ emission associated with the heat supplied by the boiler in the winter period ($E_{p,th,WD,Wi}$ and $CO_{2,th,WD,Wi}$) has a decreasing trend with the surface of the solar field;
- (5) the thermal energy provided by the boiler during summer ($E_{p,th,WD,Sum}$) insignificantly contributes to the total primary energy and equivalent CO₂ emissions when referring to systems with evacuated tube collectors (Figures 13 and 16).

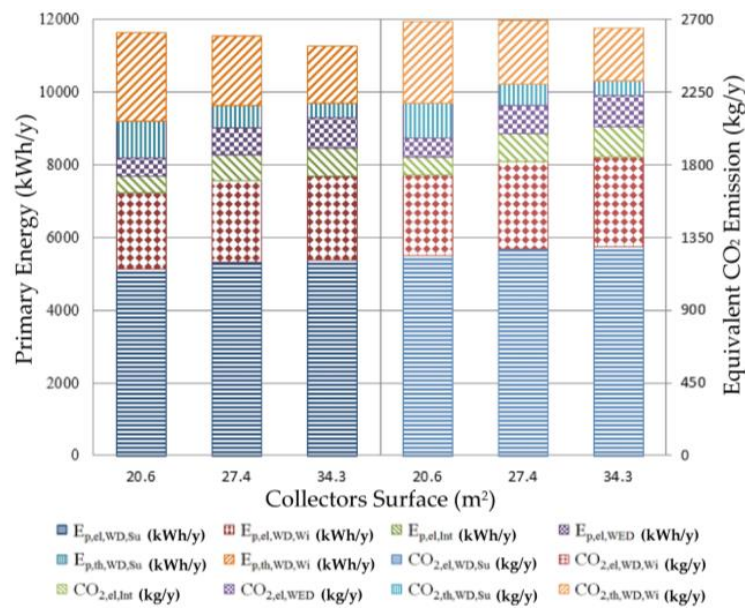


Figure 16. Annual primary energy consumption and equivalent CO₂ emission associated with seasonal electric and thermal demands for the plant with cross-flow heat recovery unit (Scenario C), evacuated tube collectors, tilt angle of 40° and 0% of solar thermal energy surplus used.

As regards economic analysis, SDEC systems are more expensive than conventional plants, mainly due to the presence of a DW, solar field and TS tank.

The Italian financial support mechanism, currently applicable to this type of renewable energy technology, establishes a contribution that depends on the surface and on the type of SC employed, but it does not take into account the typology of the solar cooling system installed (absorption, adsorption heat pumps, DEC, etc.). For the specific applications considered in this paper, it occurs that economic subsidy is too low to obtain an acceptable payback period if these systems are only used for the summer and winter air conditioning of the classroom.

If 50% of surplus solar thermal energy is exploited, the *SPB* period ranges between 25 and 9 years, with the lowest value obtained when the maximum flat-plate SC surface (about 34 m²), optimal tilt angle and pre-cooling/dehumidification coil (Scenario D) are chosen. The largest value occurs for the standard system (Scenario A) worse tilt angle and a solar field of 20 m² of flat-plate collectors.

If the total use of solar thermal energy surplus is assumed, the differences between the various scenarios reduce, and the most influential factor becomes the absorbing surface. The *SPB* ranges between 12 years (Scenario A, 20 m² of flat collectors and optimal tilt angle) and 5 years (system with pre-cooling and 34 m² of flat-plate collectors). The *SPB* period for plants with evacuated tube collectors decreases to 11 years in Scenario A with 20 m² of collectors and optimal tilt angle, while a minimum value of 6 years is obtained in Scenario D with 34 m² of collectors.

In order to summarize the best energy, environmental and economic results, Tables 7 and 8 show *PES*, ΔCO_2 and *SPB* for the four analyzed scenarios with 0%, 50% and 100% use of the solar thermal energy surplus, when the optimal configuration (surface and tilt angle) are chosen for plants with flat-plate and evacuated tube collectors, respectively. The *SPB* values for cases with 0% use of the solar thermal energy surplus are not reported because they far exceed the useful life of the plant.

Table 7. Best energy, environmental and economic results with flat-plate collectors.

Energy Surplus Used	Scenario A			Scenario B			Scenario C			Scenario D		
	PES (%)	ΔCO_2 (%)	SPB (y)	PES (%)	ΔCO_2 (%)	SPB (y)	PES (%)	ΔCO_2 (%)	SPB (y)	PES (%)	ΔCO_2 (%)	SPB (y)
0%	9.74	7.36	-	12.80	10.20	-	13.22	10.50	-	19.18	17.03	-
50%	43.38	40.13	11	45.50	42.17	10	45.77	42.37	11	49.37	45.72	10
100%	58.78	55.81	6	60.40	57.40	6	60.61	57.56	5	63.41	60.23	5

Table 8. Best energy, environmental and economic results with evacuated tube collectors.

Energy Surplus Used	Scenario A			Scenario B			Scenario C			Scenario D		
	PES (%)	ΔCO_2 (%)	SPB (y)	PES (%)	ΔCO_2 (%)	SPB (y)	PES (%)	ΔCO_2 (%)	SPB (y)	PES (%)	ΔCO_2 (%)	SPB (y)
0%	20.45	17.14	-	22.27	18.84	-	22.33	18.81	-	24.47	21.74	-
50%	58.14	54.72	13	59.44	56.00	13	59.52	56.04	13	61.05	57.47	12
100%	71.60	68.86	7	72.58	69.84	7	72.65	69.89	7	73.84	71.04	6

7. Conclusions

A desiccant-based AHU fed with a renewable energy source such as solar energy is an excellent choice for the air conditioning of buildings. Energy and environmental benefits can be achieved in comparison with conventional plants. However economic feasibility is still hard to obtain. Suitable modifications to the standard layout can deliver significant performance improvements and operating cost reductions.

In this paper, the hybrid AHU installed at University of Sannio (Italy) was modelled in TRNSYS, both in the standard configuration and by applying some modifications to reduce the thermal energy required for regeneration of the DW. The introduced modifications concern:

- the pre-heating of the regeneration air with heat recovery from chiller condenser;
- the pre-heating of the regeneration air with heat recovery from the exhaust regeneration air in a CF;
- the pre-cooling/dehumidification of the process air.

Moreover, for each configuration, different collector types (flat-plate, evacuated tube), surfaces (20–34 m²) and tilt angles (20°–55°) are considered.

Simulations of the innovative AHU, coupled to a solar field, were carried out in order to develop a thermo-economic assessment.

The obtained results show that the evacuated tube collectors improve the energy and environmental performance of the hybrid desiccant systems compared to conventional ones (up to 24% of primary energy saving with optimal tilt angle and surface) but they are more expensive than flat-plate collectors that can provide primary energy savings up to 19%, with optimal tilt angle and surface. With regards to the equivalent CO₂ avoided emissions, they range between 2.5% and 17% in the scenarios with flat-plate collectors and between 12% and 22% with evacuated tube collectors.

For both collector types, the best plant modification is the pre-cooling of the process air. A further analysis is performed, considering different use (0%–100%) of the solar thermal energy not used for air conditioning purposes and that can be used for further heating requirements. The exploitation of this surplus becomes fundamental for the achievement of acceptable SPB periods, even in the presence of economic incentives. If 50% of solar thermal energy surplus is used, the SPB period ranges between 25 and 9 years (for the standard configuration with 20 m² of flat-plate collectors and the pre-cooling modification with 34 m² of flat-plate collectors, respectively, the optimal tilt angle is assumed in the best case).

The best energy, environmental and economic results reached in the innovative plants (in particular in Scenario D) with flat-plate and evacuated tube collectors when 100% of solar surplus is used are: 63%, 60%, 5 years and 74%, 71%, 6 years respectively.

A further analysis for a future work concerns the study of plant layouts which combine the modifications presented above. Furthermore, the desiccant-based AHU could be compared with the traditional one when both are coupled with SC.

Author Contributions: All the authors have transversal expertise on the main topics of this paper (solar collectors, desiccant cooling and thermo-economic analysis), and they jointly shared the structure and aims of the manuscript. More specifically, Carlo Roselli and Francesco Tariello dealt more with the solar circuit, Giovanni Angrisani dealt more with the desiccant-based air-handling unit, Maurizio Sasso and Giuseppe Peter Vanoli contributed more to the thermo-economic analysis. Finally, all the authors equally contributed during the writing and the critical revision of the paper, according to the reviewers' comments.

Conflicts of Interest: The authors declare no conflict of interest.

Nomenclature

A	Area (m^2)
a_1	Efficiency slope ($W/(m^2 \cdot K)$)
a_2	Efficiency curvature ($W/(m^2 \cdot K^2)$)
c	Unitary cost ($\text{€}/Nm^3$) or ($\text{€}/kWh$)
C_p	Specific heat ($J/(kg \cdot K)$)
CO_2	equivalent CO_2 emission ($kg/year$)
EC	Extra cost (€)
E	Energy ($kWh/year$)
E_p	Primary energy ($kWh/year$)
F_1	F_1 potential
F_2	F_2 potential
F	Cash flow per year ($\text{€}/year$)
g	Total solar energy transmittance
G	Total incident radiation (W/m^2)
$I_{a,tot}$	Annual incentive ($\text{€}/year$)
k	Tank fluid thermal conductivity ($W/(m \cdot K)$)
m	Mass of node (kg)
MC	Annual maintenance cost ($\text{€}/year$)
mc	Specific annual maintenance cost ($\%/year$)
\dot{m}_{down}	Bulk fluid flowrate down the tank (kg/s)
\dot{m}_{up}	Bulk fluid flowrate up the tank (kg/s)
\dot{m}_{1in}	Mass flowrate entering at inlet 1 (kg/s)
\dot{m}_{1out}	Mass flowrate leaving at outlet 1 (kg/s)
\dot{m}_{2in}	Mass flowrate entering at inlet 2 (kg/s)
\dot{m}_{2out}	Mass flowrate leaving at outlet 2 (kg/s)
N	Number of years
OC	Operating costs ($\text{€}/year$)
PES	Primary energy saving ($\%$)
S	Gross solar collector area (m^2)
SPB	Simple payback (year)
t	Air temperature in Equations (4) and (5) ($^{\circ}C$)
T	Temperature (K)
T_{1in}	Temperature of the fluid entering at inlet 1 (K)
T_{2in}	Temperature of the fluid entering at inlet 2 (K)
U	Total loss coefficient ($W/m^2 \cdot K$)
V	Volume ($Sm^3/year$)

Greek Symbols

α	Specific emission factor of electricity supplied by the grid ($kgCO_2/kWh_{el}$)
β	Specific emission factor for primary related to natural gas combustion ($kgCO_2/kWh_{Ep}$)
ΔCO_2	Equivalent CO_2 avoided emission ($\%$)
Δk	De-stratification conductivity ($W/(m \cdot K)$)
ΔT	Temperature difference (K)
ΔT_{ln}	Logarithmic mean temperature difference (K)
$\Delta x_{i+1 \rightarrow i}$	Distance between node i and the node below it ($i + 1$) (m)
$\Delta x_{i-1 \rightarrow i}$	Distance between node i and the node above it ($i - 1$) (m)

ΔU	Additional loss coefficient ($W/(m^2 \cdot K)$)
η	Efficiency
η_{col}	Collector efficiency
η_0	Intercept efficiency
τ	Time (s) or (h)
ω	Air humidity ratio (g/kg)

Subscripts

a	Ambient
aux	Auxiliaries
B	Boiler
c	Cross-section area of the node
chil	Chiller
col	Collector
EG	Electric grid
el	Electric
F_1	F_1 Potential
F_2	F_2 Potential
hx	Heat exchanger
i	Generic node
in	Inlet
Int	Intermediate season
j	Generic air state
k	Generic year
NG	Natural gas
r	Generic bracket
s	Surface of the node
Su	Summer period
tank	Storage tank
th	Thermal
tot	Total
WD	Week days
WED	Weekend days
Wi	Winter period

Superscripts

AS	Alternative system
CS	Conventional system

Acronyms

AHU	Air handling unit
AS	Alternative system
B	Boiler
CC	Cooling coil
CF	Cross-flow heat exchanger
CH	Chiller
COP	Coefficient of performance
CS	Conventional system
DEC	Desiccant and evaporative cooling
DW	Desiccant wheel
EC	Evaporative cooler
EHP	Electric heat pump
HC	Heating coil
HC2	Post-heating coil
HVAC	Heating, ventilation and air conditioning systems
HW-HX	Hot water heat exchanger
SC	Solar collectors
SDEC	Solar-driven desiccant and evaporative cooling system
TS	Thermal storage

References

1. Angrisani, G.; Roselli, C.; Sasso, M.; Tariello, F. Assessment of energy, environmental and economic performance of a solar desiccant cooling system with different collector types. *Energies* **2014**, *7*, 6741–6764. [[CrossRef](#)]
2. Angrisani, G.; Roselli, C.; Sasso, M. Effect of rotational speed on the performances of a desiccant wheel. *Appl. Energy* **2013**, *104*, 268–275. [[CrossRef](#)]
3. Pennington, N.A. Humidity Changer for Air Conditioning. USA Patent No. 2700537, 25 January 1955. Available online: www.google.ch/patents/US2700537 (accessed on 21 April 2016).
4. La, D.; Dai, Y.J.; Li, Y.; Wang, R.Z.; Ge, T.S. Technical development of rotary desiccant dehumidification and air conditioning: A review. *Renew. Sustain. Energy Rev.* **2010**, *14*, 130–147. [[CrossRef](#)]
5. Collier, R.; Arnold, F.; Barlow, R. An overview of open-cycle desiccant cooling systems and materials. *J. Sol. Energy Eng.* **1982**, *104*, 28–34. [[CrossRef](#)]
6. Pesaran, A.A.; Penney, T.R.; Czanderna, A.W. Desiccant Cooling: State-of-the-Art Assessment. National Renewable Energy Laboratory: Golden, CO, USA, 1992; Available online: <http://www.osti.gov/scitech/servlets/purl/6925169> (accessed on 21 April 2016).
7. La, D.; Dai, Y.J.; Li, Y.; Ge, T.S.; Wang, R.Z. Use of regenerative evaporative cooling to improve the performance of a novel one-rotor two-stage solar desiccant dehumidification unit. *Appl. Therm. Eng.* **2012**, *42*, 11–17. [[CrossRef](#)]
8. Ge, T.S.; Dai, Y.J.; Wang, R.Z.; Li, Y. Experimental investigation on a one-rotor two-stage rotary desiccant cooling system. *Energy* **2008**, *33*, 1807–1815. [[CrossRef](#)]
9. La, D.; Li, Y.; Dai, Y.J.; Ge, T.S.; Wang, R.Z. Development of a novel rotary desiccant cooling cycle with isothermal dehumidification and regenerative evaporative cooling using thermodynamic analysis method. *Energy* **2012**, *44*, 778–791. [[CrossRef](#)]
10. La, D.; Dai, Y.; Li, Y.; Ge, T.; Wang, R. Case study and theoretical analysis of a solar driven two-stage rotary desiccant cooling system assisted by vapor compression air-conditioning. *Sol. Energy* **2011**, *85*, 2997–3009. [[CrossRef](#)]
11. Zhu, J.; Chen, W. Energy and exergy performance analysis of a marine rotary desiccant air-conditioning system based on orthogonal experiment. *Energy* **2014**, *77*, 953–962. [[CrossRef](#)]
12. La, D.; Dai, Y.J.; Li, Y.; Tang, Z.Y.; Ge, T.S.; Wang, R.Z. An experimental investigation on the integration of two-stage dehumidification and regenerative evaporative cooling. *Appl. Energy* **2013**, *102*, 1218–1228. [[CrossRef](#)]
13. Enteria, N.; Yoshino, H.; Mochida, A.; Takaki, R.; Satake, A.; Yoshie, R.; Mitamura, T.; Baba, S. Construction and initial operation of the combined solar thermal and electric desiccant cooling system. *Sol. Energy* **2009**, *83*, 1300–1311. [[CrossRef](#)]
14. Enteria, N.; Yoshino, H.; Mochida, A.; Takaki, R.; Satake, A.; Yoshie, R.; Mitamura, T.; Baba, S. Development and construction of the novel solar thermal desiccant cooling system incorporating hot water production. *Appl. Energy* **2010**, *87*, 478–486. [[CrossRef](#)]
15. Hürdoğan, E.; Büyükalaca, O.; Yılmaz, T.; Hepbaşlı, A. Experimental investigation of a novel desiccant cooling system. *Energy Build.* **2010**, *42*, 2049–2060. [[CrossRef](#)]
16. Chung, J.D.; Lee, D.Y. Contributions of system components and operating conditions to the performance of desiccant cooling systems. *Int. J. Refrig.* **2011**, *34*, 922–927. [[CrossRef](#)]
17. Enteria, N.; Yoshino, H.; Mochida, A.; Satake, A.; Yoshie, R.; Takaki, R.; Yonekura, H.; Mitamura, T.; Tanaka, Y. Performance of solar-desiccant cooling system with Silica-Gel (SiO₂) and Titanium Dioxide (TiO₂) desiccant wheel applied in East Asian climates. *Sol. Energy* **2012**, *86*, 1261–1279. [[CrossRef](#)]
18. Zang, R. T Dynamic Optimization of Integrated Active-Passive Strategies for Building Enthalpy Control. Ph.D. Thesis, Carnegie Mellon University, Pittsburgh, PA, USA, May 2014.
19. Ghali, K. Energy savings potential of a hybrid desiccant dehumidification air conditioning system in Beirut. *Energy Convers. Manag.* **2008**, *49*, 3387–3390. [[CrossRef](#)]
20. Sheng, Y.; Zhang, Y.; Sun, Y.; Fang, L.; Nie, J.; Ma, L. Experimental analysis and regression prediction of desiccant wheel behavior in high temperature heat pump and desiccant wheel air-conditioning system. *Energy Build.* **2014**, *80*, 358–365. [[CrossRef](#)]

21. Elzahzby, A.M.; Kabeel, A.E.; Bassuoni, M.M.; Abdelgaied, M. Effect of inter-cooling on the performance and economics of a solar energy assisted hybrid air conditioning system with six stages one-rotor desiccant wheel. *Energy Convers. Manag.* **2014**, *78*, 882–896. [[CrossRef](#)]
22. Angrisani, G.; Minichiello, F.; Roselli, C.; Sasso, M. Desiccant HVAC system driven by a micro-CHP: Experimental analysis. *Energy Build.* **2010**, *42*, 2028–2035. [[CrossRef](#)]
23. Calise, F.; Dentice d’Accadia, M.; Roselli, C.; Sasso, M.; Tariello, F. Desiccant-based AHU interacting with a CPVT collector: Simulation of energy and environmental performance. *Sol. Energy* **2014**, *103*, 574–594. [[CrossRef](#)]
24. *Ergonomics of the Thermal Environment—Analytical Determination and Interpretation of Thermal Comfort Using Calculation of the PMV and PPD Indices and Local Thermal Comfort Criteria*; ISO 7730; International Standard: Geneva, Switzerland, 2005.
25. *Prestazione Energetica Degli Edifici-Requisiti Energetici per Illuminazione (Energy Performance of Buildings—Energy Requirements for Lighting)*; UNI EN 15193; Italian Standard: Rome, Italy, 2008. (In Italian)
26. Mardiana, A.; Riffat, S.B. Review on physical and performance parameters of heat recovery systems for building applications. *Renew. Sustain. Energy Rev.* **2013**, *28*, 174–190. [[CrossRef](#)]
27. Henning, H.M.; Pagano, T.; Mola, S.; Wiemken, E. Micro tri-generation system for indoor air conditioning in the Mediterranean climate. *Appl. Therm. Eng.* **2007**, *27*, 2188–2194. [[CrossRef](#)]
28. Angrisani, G.; Minichiello, F.; Roselli, C.; Sasso, M. Experimental analysis on the dehumidification and thermal performance of a desiccant wheel. *Appl. Energy* **2012**, *92*, 563–572. [[CrossRef](#)]
29. Angrisani, G.; Roselli, C.; Sasso, M.; Tariello, F. Dynamic performance assessment of a micro-trigeneration system with a desiccant-based air handling unit in Southern Italy climatic conditions. *Energy Convers. Manag.* **2014**, *80*, 188–201. [[CrossRef](#)]
30. Solar Energy Laboratory. *TRNSYS 17, a TRAnSient System Simulation Program*; University of Wisconsin: Madison, WI, USA, 2010.
31. *Thermal Energy System Specialists Components Library v. 17.01*; Thermal Energy System Specialists: Madison, WI, USA, 2004.
32. Angrisani, G.; Roselli, C.; Sasso, M. Experimental validation of constant efficiency models for the subsystems of an unconventional desiccant-based Air Handling Unit and investigation of its performance. *Appl. Therm. Eng.* **2012**, *33–34*, 100–108. [[CrossRef](#)]
33. Angrisani, G.; Canelli, M.; Roselli, C.; Sasso, M. Calibration and validation of a thermal energy storage model: Influence on simulation results. *Appl. Therm. Eng.* **2014**, *67*, 190–200. [[CrossRef](#)]
34. Duffie, J.A.; Beckmann, W.A. *Solar Engineering of Thermal Processes*, 3rd ed.; John Wiley & Sons: New York, NY, USA, 2006; pp. 238–323.
35. Jurinak, J.J. Open Cycle Solid Desiccant Cooling: Component Models and System Simulations. Ph.D. Thesis, University of Wisconsin, Madison, WI, USA, 1982.
36. TERNA, Statistiche e Previsioni, Dati Statistici, Produzione, 2011. Available online: <http://www.terna.it/archiviadocumenti.aspx> (accessed on 21 April 2016). (In Italian)
37. TERNA, Nota di Sintesi, Dati Statistici Sull’energia Elettrica in Italia, 2011. Available online: <http://www.terna.it/archiviadocumenti.aspx> (accessed on 21 April 2016). (In Italian)
38. AEEG (Autorità per l’Energia Elettrica e il Gas Direzione Mercati), Revisione dei Fattori di Perdita di Energia Elettrica, Applicati All’energia Elettrica Immessa Nelle Reti di Media e Bassa Tensione 2012. Available online: <http://www.autorita.energia.it/allegati/docs/12/013-12.pdf> (accessed on 21 April 2016). (In Italian)
39. Caputo, A. Fattori di Emissione di CO₂ nel Settore Elettrico e Analisi Della Decomposizione Delle Emissioni, 2012; Available online: http://www.isprambiente.gov.it/files/pubblicazioni/rapporti/rapporto_172_2012.pdf (accessed on 21 April 2016). (In Italian)
40. Sabiha, M.A.; Saidur, R.; Mekhilef, S.; Mahian, O. Progress and latest developments of evacuated tube solar collectors. *Renew. Sustain. Energy Rev.* **2015**, *51*, 1038–1054. [[CrossRef](#)]

